# A theoretical/experimental approach to the intrinsic oxidation reactivities of C/C composites and of their components

J. Lachaud *, N. Bertrand, G. L. Vignoles, G. Bourget, F. Rebillat, and P. Weisbecker

*Université Bordeaux I*
*Laboratoire des Composites ThermoStructuraux (LCTS)*
*3, Allée de La Boétie, 33600 Pessac, France*

**Abstract**

The oxidation reactivities of two C/C composites and of their available components (fibers, bulk matrices) are determined by measurement of mass loss rate in a cylindrical oxidation reactor under dry air and at atmospheric pressure. In order to identify reactional and diffusional regimes, and to provide a safe method for the identification of the intrinsic heterogeneous reaction rates at high temperatures, a modeling approach has been developed. Diffusion of the oxidant is considered throughout the reactor for all the samples (global-scale modeling) in combination with convection and reactions. Fibers have been arranged in unidirectional bundles in which diffusion is also considered (local-scale modeling). The importance of the reaction rate relatively to global-scale and local-scale diffusion has been evaluated. When reaction is slow enough, diffusion effects can be neglected; in the converse case, the intrinsic reaction rates are extracted from the experimental data using the models. Incidentally, the comparison of the fiber and matrix intrinsic reactivities supports the idea that the composites feature a complex oxidation behavior mainly based on a weakest link process. This result is illustrated and discussed using SEM and TEM investigations.

## 1 Introduction

Carbon/Carbon (C/C) composites, which keep excellent mechanical properties at high temperatures [1], are used in various applications such as atmospheric re-entry (thermal protection systems), propulsion (rocket nozzles), and aeroplane braking (disks) [2]. However, in these applications, C/C composites are ablated by oxidation or even sublimation in the case of re-entry [3]. Thus, an accurate evaluation of the wall recession caused by ablation is useful for structure design. Hence, the coupled physical phenomena leading to carbon loss and resulting in a global surface recession have to be known. Namely, during ablation, C/C composites develop surface roughness features [4, 5], which display a strong coupling with the surrounding environment [3, 6]. Some recent models [5, 7–9] have shown that the surface roughness might

* Corresponding author. *Fax:* +33 556 841 225. *E-mail address:* jean.lachaud@gadz.org (J. Lachaud)

arise from the heterogeneity of the composites, whose fibers and matrices are made of distinct forms of carbon. Therefore, in order to efficiently address the global study of ablation and to provide a theoretical interpretation for surface roughness onset, an accurate knowledge of both the composite reactivity and the intrinsic reactivities of the composite components are useful. This work aims to furnish such data in the case of oxidation.

Literature data on oxidation show that experimental values of reactivities under apparently similar conditions may differ by a factor ten [10–13]; the causes of the discrepancy are well known [1]: catalytic effects, different thermal treatments of a same material, experimental variations (gas velocity, quality of the air, configuration of the reactor, diffusion effects). Consequently, it appears that reactivity measurements have to be done on the materials of the study themselves paying special attention to the material history, and that the experimental conditions should be perfectly mastered, or even modeled, and similar for all samples. This work proposes to do so. The experimental approach is coupled to a theoretical approach in order to extract from the raw experimental values the intrinsic oxidation reactivities, even when diffusion effects are not negligible.

Thermogravimetric analysis (TGA) reactors are the most convenient ones to study oxidation rates because they enable a continuous *in situ* measurement of mass loss [11, 12, 14–17]. For the materials of this study, plots of the experimental oxidation rates versus temperature show a slope change around $873\,K$ [14, 17, 18] due to a mass transfer limitation [19]. Therefore, the intrinsic reactivities cannot be assessed for temperatures higher than $873\,K$ in TGA. Moreover, for lower temperatures, even if diffusion effects are not predominant, they tend to lower the apparent oxidation rate in a proportion that is difficult to evaluate. Consequently, in this work, the use of another setup is proposed: an oxidation reactor, which has been designed on purpose. Naturally, diffusional limitations may appear as well in this reactor, and have to be taken into account. However, a more appropriate geometry and a larger possible gas flow rate favor a thinner dynamic boundary layer above the sample. This increases the oxygen mass transfer to the wall and the transition temperature that characterizes the onset of the diffusion-limited regime, so that useful measurements may be conducted up to $898\,K$ for all the materials of this study. In addition to this, the geometry has been designed to enable a detailed computational fluid dynamics (CFD) modeling which helps in evaluating diffusion effects and in providing a truly intrinsic oxidation rate.

This document is divided in four sections. The first section addresses the materials, experimental conditions and protocol. The second section describes a theoretical approach developed to extract intrinsic reactivities from raw experimental values, based on a 3D CFD modeling of the reactor and an original method to assess the intrinsic fiber reaction rate from a bundle apparent rate, even when diffusive effects are not negligible. Finally, the obtained values are discussed in regard to literature data and material architectures.

## 2 Experiments

### *2.1 Materials*

Two C/C composites are studied : (i) a 3D C/C composite, graphitized at $2300°C$ for 24 hours in a laboratory furnace, and made from a 3-D preform of ex-PAN carbon fibers, named $F1$, and a matrix of pitch-based carbon, named $M1$, and (ii) a 2D carbon/resin composite (2D C/R) pyrolyzed at $1400\,°C$ for 12 hours, and made from ex-cellulose carbon fibers, $F2$, and a phenolic resin, called $M2$ under its pyrolyzed form. The composite components are available separately. Concerning the fibers, $F1$ and $F2$ have also been respectively treated at $2300°C$ for 24 hours and at $1400\,°C$ for 12 hours. To furnish a larger data set, to permit comparison of the values of the oxidation rates with those of well-known commercial fibers, and to quantify thermal treatment effects, other fibers from other precursors have been oxidized. Two forms of $P100$ ex-pitch fibers are tested : (i) raw ($F3-R$) (ii) treated at $1400\,°C$ for one hour ($F3-T$). Three forms of T300 ex-PAN fibers are tested : (i) raw ($F4-R$), (ii) treated at $1400\,°C$ for one hour ($F4-T$), (iii) $F4-G$ : treated at high temperature ($2300°C$). Concerning the matrices, $M2$ is easy to obtain by pyrolysis of a phenolic resin. Due to the high pressures and temperatures required to fabricate the 3D C/C, a matrix representative of $M1$ can only be obtained using the 3D C/C fabrication process. Bits of the 3D C/C matrix have been isolated from the crust of the coarse material at different processing stages : (i) carbonized ($M1-C$), (ii) graphitized ($M1-G$). All the samples except raw fibers have been treated at $1400\,°C$ for one hour in order to vaporize surface alkaline impurities that are known to strongly catalyze oxidation [12]. This treatment is useful to guarantee that the sample surface, that can have been affected by finger sweat deposition, is clean before oxidation tests. No structural ordering occurs at this temperature since all the materials have been previously fabricated or treated at higher temperatures.

### *2.2 Oxidation reactor*

The oxidation reactor is a cylindrical tube, heated resistively; the lower half of the tube is occupied by a semi-cylindrical refractory block. The sample is placed in a $1\,cm^3$ cubic crucible, incorporated in the center of the lower wall of the inner part of reactor (see figure 1). The effective reactive surface of the sample is thus reduced to a $1\,cm^2$ square surface. The cubic crucible, made of quartz, does not display any catalytic effect on oxidation reaction. The composites and the pitch-based matrix are dense materials which are machined at crucible size and inserted in the crucible. The pyrolyzed phenolic resin, which is very porous, is ground and its powder is placed in the crucible. As represented at figure 2-a, the fibers are arranged in dense unidirectional bundles in the crucible.

Dry air at atmospheric pressure is injected in the first part of the reactor (not represented on figure 1) where it is pre-heated and homogenized by using a gas diffuser. The inner temperature of the reactor ($898\,K$) is controlled using micro-controllers linked to a K-type thermocouple.

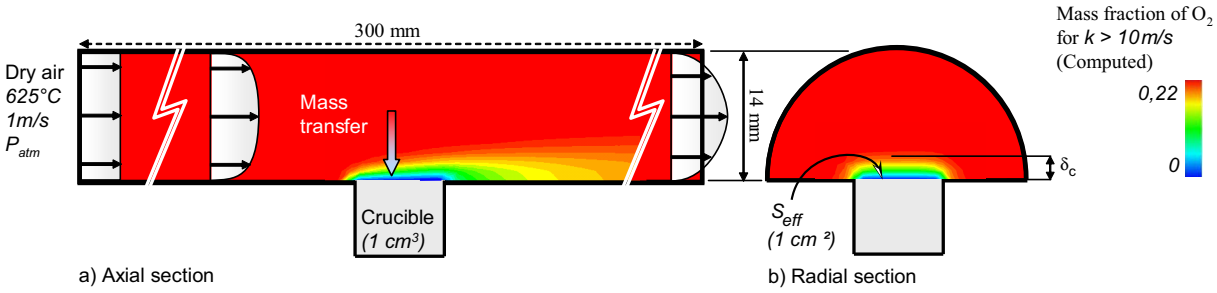


Fig. 1. Oxidation reactor geometry and experimental conditions (dry air, $T = 898\,K$, $P = 1atm$).

The hot air flow velocity over the sample is $1\,m/s$. This value is a compromise ensuring both laminar flow conditions and a high oxygen mass transfer. The air flow velocity is conveniently mastered in standard conditions using a ball flowmeter, and extrapolated using the perfect gas law. The air flow corresponding to the retained velocity is $400$ standard liters per hour. The crucible containing the sample is regularly extracted from the reactor and weighted to follow mass loss. It has been verified that this operation does not disturb the oxidation process by comparing the results to that of experiments for which the samples were just extracted once.

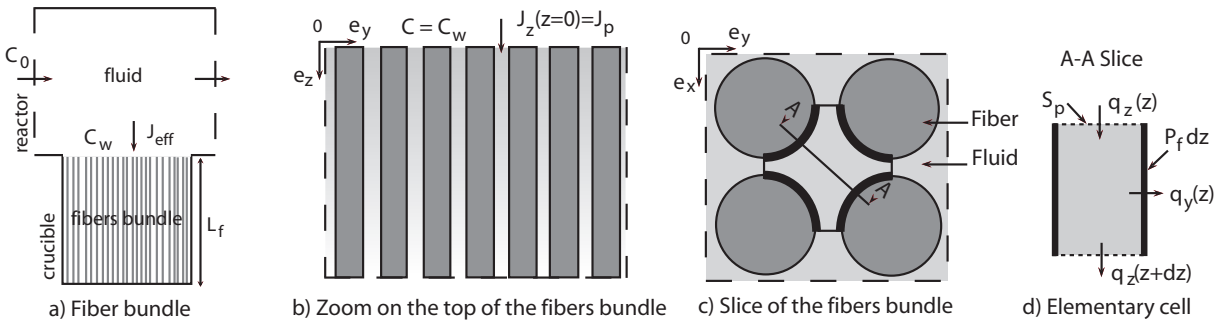


Fig. 2. Sketch of a unidirectional bundle of cylindrical fibers placed in a crucible

### *2.3 Experimental results*

The experimental results are given in table 1 for each sample. The intrinsic density ($\rho_i$) is obtained by helium pycnometry. The initial mass of the samples is $m_0$.

To clearly situate this work in the general context of the studies on C/C composites behavior, the interest of the more classical definitions of oxidation rates should be discussed. The overall oxidation rate $r$ ($g.g^{-1}.s^{-1}$) is often obtained by the following equation [16]:

$$r = -\frac{1}{m_j}\left(\frac{dm}{dt}\right) \tag{1}$$

where $m_j$ is the mass of the sample either at initial time ($m_0$) or after a given burn-off level at time $t$ ($m$) and $dm/dt$ is the instantaneous mass loss. This definition of $r$ is strongly correlated

to the samples geometry and porosity [18]; hence, it is convenient for the comparison of similar samples in different experimental conditions (oxidation temperature [20, 21], gas composition or pressure [21]) or with specific treatments (antioxidation treatments [18,20,21], thermal treatments [14]). For a specific analysis of a material, two oxidation rates (in $g.m^{-2}.s^{-1}$) are usually determined from $r$: the specific rate $j_s$ and the intrinsic rate $j_i$, respectively given by the following equations : $j_s = r/TSA$, $j_i = r/ASA$ [15, 16]. TSA (in $m^2.g^{-1}$) is the total surface area per mass unit determined for example by Krypton adsorption at $77\,K$ (BET method) [16]. As far as composite behavior is concerned, $j_s$ is biased in general as the the TSA measured by BET is definitely a total surface area, that is, including the whole surface accessible to krypton, while during oxidation, because of mass transfer limitation, oxygen cannot reach the whole accessible surface in the general case [19]. The studies have then to be restricted to reaction-limited regime in the pores. Interestingly, in this regime, it has been shown that the specific reactivity of a 3D C/C composite was not an additive property with respect to that of its components [15]. ASA (in $m^2.g^{-1}$) is the active surface area, a macroscopic value introduced to link the local notion of active site to the overall reactivity of carbon surfaces [22]. Active sites are places where chemisorption can occur, that is, where the graphene planes present some defects [23]. The ASA measurement may rely, among others, on oxygen sorption and $CO$/$CO_2$ thermodesorption at low temperatures [16]. Thus, as for $j_s$, $j_i$ is only valuable to study the reaction limited-regime. It is an intrinsic oxidation rate related to the active sites activity of the total surface accessible to $O_2$. It depends on the nature of the carbon material and on the oxidizing environment, but interestingly it is nearly constant for burn-off values ranging between $0$ and $12\%$ [16]. Moreover, the intrinsic reactivity of a C/C composite made of ex-PAN fibers and pitch-based matrix has been shown to be an additive property of the reactivities of its components [16]. As a conclusion, these elaborate intrinsic reactivities cannot be directly correlated to the overall behavior of the material (recession rate, surface roughness onset), mainly in diffusional regime inside the pores. Paradoxically, to feed the ablation models, the apparent geometrical oxidation rate $j_g$ [10, 18, 20] that gives an access to the intrinsic geometrical reactivity (see section 3) seems more appropriate. It is defined as the mass loss rate per unit of geometrical surface $S_{eff}$ :

$$j_g = -\frac{1}{S_{eff}}\left(\frac{dm}{dt}\right) \tag{2}$$

The intrinsic geometrical reactivity enables to analyze and model the geometrical evolutions of the surface roughness of the composites, which is strongly linked to their behavior [7, 9, 24]. To simplify the study, it has been chosen to protect five out of six faces of the samples by including them in a crucible. The samples are then oxidized through the $1\,cm^2$ square upper surface (see figure 1). The steady state value of $j_g$, noted $j_{exp}$, is assessed for $30\%$ burn off. Indeed, for all the samples, a steady oxidation rate has been reached at that stage.

Table 1
Experimental results and theoretical exploitation (dry air, $T = 898\,K$, $P = 1atm$)

| Sample | $\rho_i$ | $m_0$ | $j_{exp}$ | $k_{eff}$ | $R_f$ | $\bar{d}_p$ | $k_f$ | Regime | |
|---|---|---|---|---|---|---|---|---|---|
| Reference | $(kg.m^{-3})$ | $(mg)$ | $(g.m^{-2}.s^{-1})$ | $(m.s^{-1})$ | $(\mu m)$ | $(\mu m)$ | $(m.s^{-1})$ | $Da$ | $\Phi$ |
| 3D C/C | 2.08 | 1504 | 0.095 | $\mathbf{3.0\,10^{-3}}$ | - | - | - | 0.039 | - |
| 2D C/R | 1.94 | 1038 | 1.31 | $\mathbf{8.5\,10^{-2}}$ | - | - | - | 1.1 | - |
| M1-C | 1.92 | 974 | 0.25 | $\mathbf{8.7\,10^{-3}}$ | - | - | - | 1.1 | - |
| M1-G | 2.12 | 940 | 0.080 | $\mathbf{2.5\,10^{-3}}$ | - | - | - | 0.032 | - |
| M2 | 1.97 | 714 | 0.64 | $\mathbf{2.6\,10^{-2}}$ | - | - | - | 0.34 | - |
| F1 | 1.85 | 463 | 0.30 | $1.0\,10^{-2}$ | 3.5 | 28 | $\mathbf{1.2\,10^{-5}}$ | 0.13 | 1.1 |
| F2 | 1.60 | 312 | 0.96 | $4.8\,10^{-2}$ | 3.5 | 37 | $\mathbf{2.1\,10^{-4}}$ | 0.62 | 4.1 |
| F3-R | 2.16 | 522 | 0.41 | $1.5\,10^{-2}$ | 5.5 | 45 | $\mathbf{3.3\,10^{-5}}$ | 0.19 | 1.5 |
| F3-T | 2.16 | 341 | 0.27 | $9.5\,10^{-3}$ | 5.5 | 74 | $\mathbf{2.6\,10^{-5}}$ | 0.12 | 1.0 |
| F4-R | 1.79 | 844 | 0.95 | $4.7\,10^{-2}$ | 3.5 | 12 | $\mathbf{1.1\,10^{-4}}$ | 0.61 | 5.2 |
| F4-T | 1.79 | 579 | 0.44 | $1.6\,10^{-2}$ | 3.5 | 20 | $\mathbf{1.8\,10^{-5}}$ | 0.21 | 1.6 |
| F4-G | 1.96 | 368 | 0.097 | $2.7\,10^{-3}$ | 3.5 | 35 | $\mathbf{3.0\,10^{-6}}$ | 0.03 | 0.51 |

## 3 Identification of intrinsic reactivities

The measured rate $j_{exp}$ is marred by diffusion effects: it is more or less lowered by mass transfer limitation as compared to the intrinsic geometrical oxidation rate. The purpose of the CFD modeling is to uncorrelate reactivity and diffusion effects in order to assess the intrinsic reactivity. For the global scale modeling, the effective geometrical reactivity $k_{eff}$ of a sample of $1\,cm^3$ placed in the crucible may be considered as the reactivity of a flat effective surface $S_{eff}$ placed on the top of the crucible and leading to the same mass loss rate:

$$\frac{dm}{dt} = -j_{exp} S_{eff} = -k_{eff} \mathcal{M}_c S_{eff} C^n \tag{3}$$

where $C$ is the oxidative species concentration ($mol.m^{-3}$), $n$ is a reaction order, and $\mathcal{M}_c$ is the molar mass of carbon ($g.mol^{-1}$). The wall recession of the materials is low enough to be neglected. The intrinsic geometrical reactivities are then equal to the effective reactivities in the case of the composites and matrices. On the other hand, this is not the case for fiber bundles, for which a porous medium approach is presented at section 3.2. The necessary evaluation of $k_{eff}$ is presented in the following section.

### *3.1 Modeling of the oxidation reactor*

The hypotheses of the global model are as follows :

(1) According to thermochemical data, at $898\,K$, under dry air and at atmospheric pressure, the chemical balance of the oxidation process writes [25]:

$$C_{(s)} + O_2 \rightleftharpoons CO_2 \tag{4}$$

In the conditions described above, this reaction is thermodynamically promoted since $\Delta_f G^\circ(CO_2) = -395\,kJ.mol^{-1}$. The equilibrium partial pressures of reactants and products are in the ratio : $P_{CO_2}/P_{O_2} = 10^{23}$ [25]. This implies that : (i) only the kinetic aspect of the reaction has to be taken into account, (ii) the reaction may be limited by a low partial pressure of $O_2$. Studies on active site reactivity have shown that the reaction order $n$ depends on many parameters like temperature, pressure or carbon crystallinity [12]. The proposed values of $n$ lie between $0.5$ and $1$ [10]. Considering the ablation modeling as a whole, the chosen value is not an issue as long as it is maintained consistently in the further modeling developments [5]. In the following, a first-order oxidation process is considered. Thus, equation (3) rewrites : $r_{exp} = \mathcal{M}_c k_{eff} C_{O_2}$ ($g.m^{-2}.s^{-1}$), with $k_{eff}$ ($m.s^{-1}$) and $C_{O_2}$ ($mol.m^{-3}$) the oxygen concentration at the surface.

(2) The surface recession, which is slow as compared to mass transfer, and low at any time, is neglected.

(3) The flow is supposed laminar. Indeed, the Reynolds number evaluated assuming a flow in a circular tube is found to lie around $300$, while the onset of turbulence appears for values around $2300$ [26].

(4) Experimental measurements using thermocouples have shown that the reactor and the sample could be considered isothermal. The hot ($898\,K$) laminar dry air flow is modeled using Navier-Stokes equations with the incompressible flow hypothesis since $v < Mach\,0.2$ [9].

(5) Multi-component mass transfer is taken into account, the species being oxygen, nitrogen, and carbon dioxide.

The inner part of the reactor is accurately modeled in 3D, its geometry is represented on figures 1 and 3. The boundary conditions are:

(1) Inlet : $T = T_0 = 898\,K$, mass fraction of oxygen in dry air : $0.222$, dry air velocity : $1\,m.s^{-1}$ with a flat profile;

(2) Outlet : $P = P_{atm}$;

(3) Walls : $T = T_0$, heterogeneous reaction on $S_{eff}$, no slip condition.

The numerical simulations of gas flow and reactant species distribution in the experimental setup have been performed with a commercial software package, *Fluent6*. Steady-state solution was attained by a first resolution of the single Navier-Stokes equations, then followed by a coupled resolution of the Navier-Stokes and species balance equations including the heterogeneous reaction. Figure 3-b shows the geometry of the mesh, which has been optimized to favor a quick convergence : it features $122,200$ hexahedral cells and $124,313$ nodes. The quality of

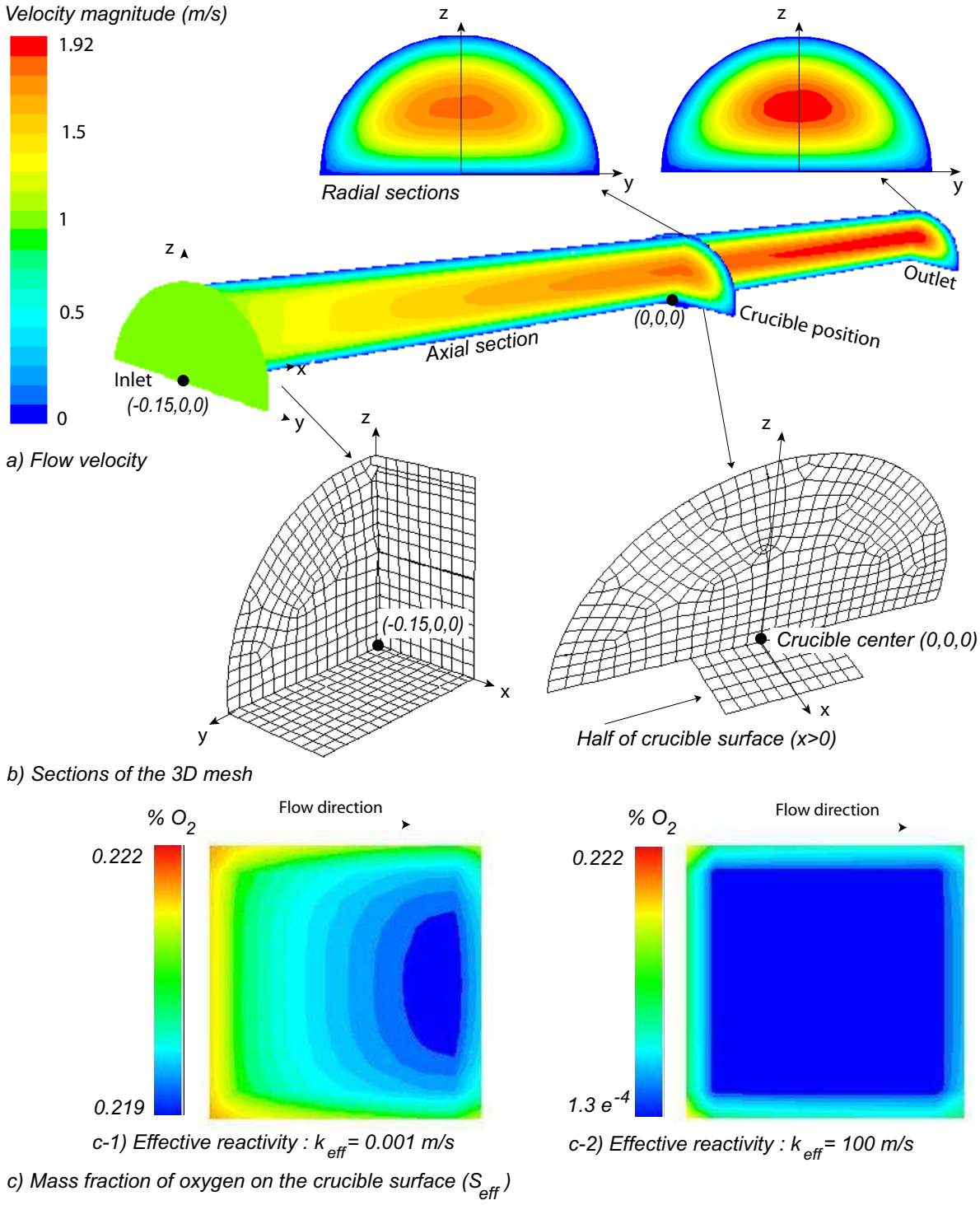


Fig. 3. 3D numerical simulation results

all elementary cells is acceptable (low distortion).

The first non-trivial result arising from this modeling is that the effect of mass transfer on the dynamic flow is not significant, even in diffusion-limited regime. On figure 3-a, the velocity

profile of the air flow is represented on an axial section and on three radial sections (inlet, crucible position, outlet). As expected, the no slip condition being respected, the viscous effects lead first to a hydrodynamic entrance region, in which a dynamic boundary layer develops from the wall to the inviscid flow region; the corresponding velocity profile displays then two parts : a parabolic part (viscous effects), and a flat part (inviscid flow). Here, the sample has been placed in the hydrodynamic entrance region. As far as mass transfer is concerned, this is beneficial since the concentration boundary layer $\delta_c$ (see figure 1) is then lower in this region [9, 26]. The maps of figure 1 show that the concentration boundary layer over the sample has a size of approximatively $2\,mm$. Figure 3-c shows that the oxygen concentration on the reacting surface ($S_{eff}$) is nearly homogeneous in all the regimes. The average molar concentration of oxygen on the reactive surface is estimated after surface integration of oxygen molar fraction. The effective mass flow consumption of carbon per surface unit and time is then calculated versus the effective oxidation rate. The result of this numerical approach is plotted on figure 4.

The mass Péclet number is low in the concentration boundary layer, that is, mass transport by convection is negligible when compared to mass transfer by diffusion. Under this hypothesis, the shape of the concentration field shows that mass transfer is mainly vertical over the sample. Hence, a 1D analytical model may help in setting up a continuous approximation of the numerical points. Considering the diffusion of oxygen in air at $898\,K$ in 1D, the effective mass flow is of the form [5, 9]:

$$j_{eff} = j_0 \frac{1}{1 + \dfrac{D}{\delta_c\, k_{eff}}} \tag{5}$$

where $j_0 = DC_0\mathcal{M}_c/\delta_c$ is the maximal mass loss obtained in diffusion-limited regime. $D$ is the diffusion coefficient of oxygen in air at $898\,K$; it is about $1.34\,10^{-4}\,m^2.s^{-1}$. $C_0$ is the oxygen concentration at inlet position, its value is $2.713\,mol.m^{-3}$. According to the numerical points represented on figure 4, one has $j_0 = 2.515\,g.m^{-2}.s^{-1}$. Hence, one deduces that $\delta_c = 1.73\,mm$. The 1D approximation of $j_{eff}$ fits well the numerical results (see figure 4). In diffusion-limited regime and in reaction-limited regime, the approximation to the numerical solution is excellent. In intermediate regime, the error is lower than $6\%$. This approximation is preferable to any linear interpolation between the numerical points. Equation (5) is used to derive the effective reactivity $k_{eff}$, free of diffusional effects, from the experimental oxidation rate $j_{exp}$ (see table 1). The second Damköhler number $Da = \delta_c\, k_{eff}/D$ that gives an evaluation of diffusional effects is also reported in table 1. In reaction-limited regime, $Da$ is small ($< 0.01$); conversely it is high in diffusion-limited regime ($> 100$). The oxidation reactor of this study had been designed to prevent diffusional effects from limiting the reaction. This objective has been reached since the experiments have been carried out in transition regime ($0.03 < Da < 6$).

### *3.2 Modeling of fiber bundle*

The aim of this part is to derive $k_f$ (in $m.s^{-1}$), the actual oxidation rate of the fibers, from $k_{eff}$, the effective reaction rate of a fiber bundle, which is the accessible data at global scale. The approach is similar to the work that P. L. Walker [19] developed for porous carbons, but with a more controlled pore morphology. Indeed, the modeling of the fiber bundle, which is a porous medium, must be feasible with a good accuracy and a sufficient mass has to be placed in the crucible to enable an accurate mass loss measurement. Therefore, the main difficulty is to find a suitable way to arrange the fibers. The retained solution is as follows. A fiber bundle, made of approximatively 600,000 fibers, is vertically included in the square crucible (see figure 2-a). The local porosity of the bundle is homogeneous and the tortuosity is negligible along the $\mathbf{e_z}$ axis (see figure 2-b).

Carbon fibers are assumed homogeneous and isotropic. The chemical reactions are restricted to the fiber surface. The oxidation process is as described in section 3.1. The local impinging molar flux density is given by $J_y(z) = k_f C(z)$, with C(z) (in $mol.m^{-3}$) the oxygen concentration at depth $z$ (see figure 2). Mass loss is strongly coupled to mass transfer between the fluid phase

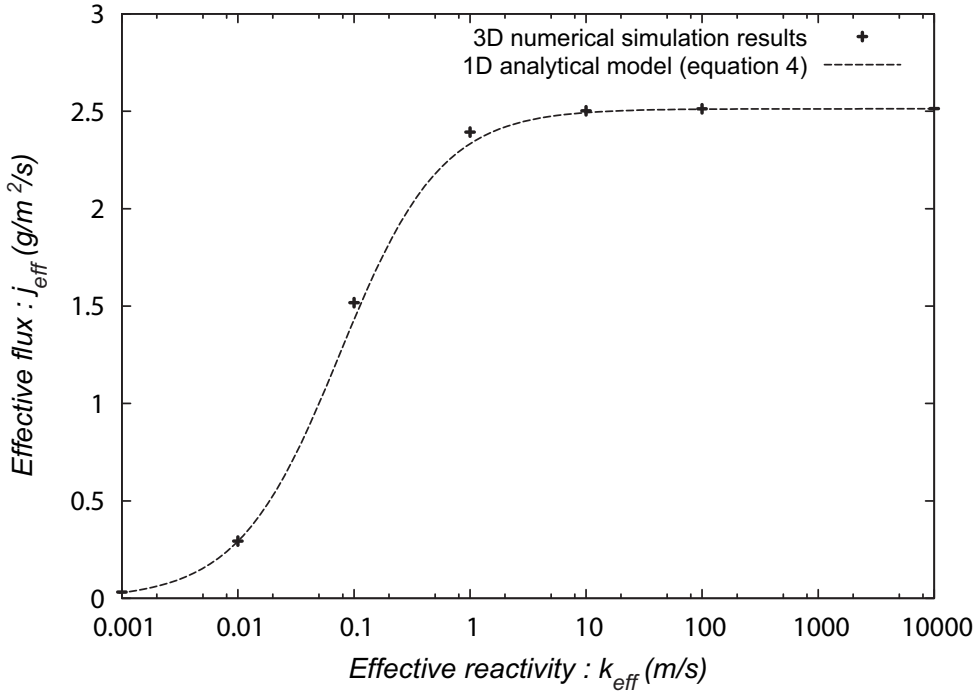


Fig. 4. Effective flux as a function of effective reactivity : comparison of 1D analytical and 3D numerical results.

and the wall. Assuming cylindrical fibers, the mean pore size writes:

$$\overline{d_p} = \frac{4\overline{S_p}}{\overline{P_f}} = \overline{d_f}(v_c\mu_f/m_f - 1) \tag{6}$$

where $\overline{d_f}$ (resp. $\overline{P_f}$) is the mean fiber diameter (resp. perimeter), $\overline{S_p}$ the mean horizontal section of the pores, $v_c$ the crucible volume, $\mu_f$ the fiber mass volume, and $m_f$ the fiber mass. The value of $\overline{d}_p$ reported in table 1 takes into account the fiber radius reduction after $30\%$ burn-off.

At $898\,K$ in dry air at atmospheric pressure, the mean free path value for oxygen is $\lambda \simeq 0.2\,\mu m$. For the bundles described above, $\overline{d}_p$ is larger than $12\,\mu m$ (table 1). Hence, the Knudsen number is low ($Kn \sim 0.01$); it characterizes bulk diffusion [27]. As the mass Péclet number is also low inside the fiber bundles, mass transfer is restricted to ordinary diffusion of oxygen in air. The mass balance in the elementary cell represented on figures 2-c and 2-d writes $q_z(z) - q_z(z+dz) = q_y(z)$. Neglecting transient effects, one has:

$$-D\nabla(C(z) - C(z+dz))S_p = k_f C(z) P_f dz \tag{7}$$

Summing up, $C(z)$ is given by the following differential equation:

$$\frac{d^2C(z)}{dz^2} - \frac{4k_f}{\overline{d_p}D}C(z) = 0 \tag{8}$$

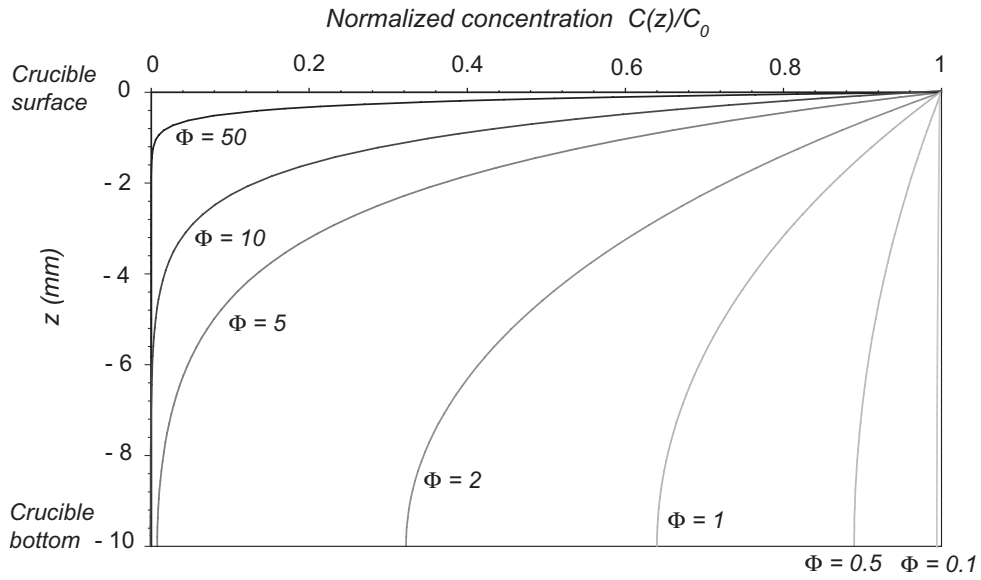


Fig. 5. Normalized concentration gradient in a fiber bundle as a function of $\Phi$.

where the boundary conditions are $C(z=0) = C_0$ and $\frac{dC}{dz}(z = L_f) = 0$.

After integration, the oxygen concentration inside the porous medium is found to be:

$$C(z) \;=\; C_0 \,\frac{\cosh\left(\,\Phi\;\left(z/L_f - 1\right)\right)}{\cosh\Phi} \tag{9}$$

where $\Phi = L_f/L$ is the Thiele number, with $L = \sqrt{\frac{\overline{d_p}D}{4k_f}}$. The normalized concentration gradient $C(z)/C_0$ in the fiber bundle is plotted on figure 5 for various values of $\Phi$. It can be shown straightforwardly that the mass loss on the top of the cylindrical fibers is negligible in front of that on the side of the fibers when the oxygen penetration in the bundle is higher than five times the fiber radius. The plot of figure 5 and the values of $\Phi$ reported in table 1 confirm *a posteriori* that this hypothesis is valid. According to this hypothesis, $J_{eff}$ and the flux that penetrates in the porous media $J_p$ (see figures 2-a and b) are linked by the relation:

$$J_p = J_{eff}\,\frac{S_{eff}}{\overline{S}_p} = J_{eff}\,\frac{1}{1 - m_f/(L_f\rho_f S_{eff})} \tag{10}$$

At the surface ($z = 0$), the divergence of $J_p$ is null. Then, Fick's first law gives:

$$J_p \;= D\,\frac{dC}{dz}\Big|_{z=0} \;=\; \frac{DC_0}{L}\tanh(\Phi) \tag{11}$$

Substituting the relation $J_{eff} = k_{eff}C_w$ in equation (10), and combining this latter with equa-

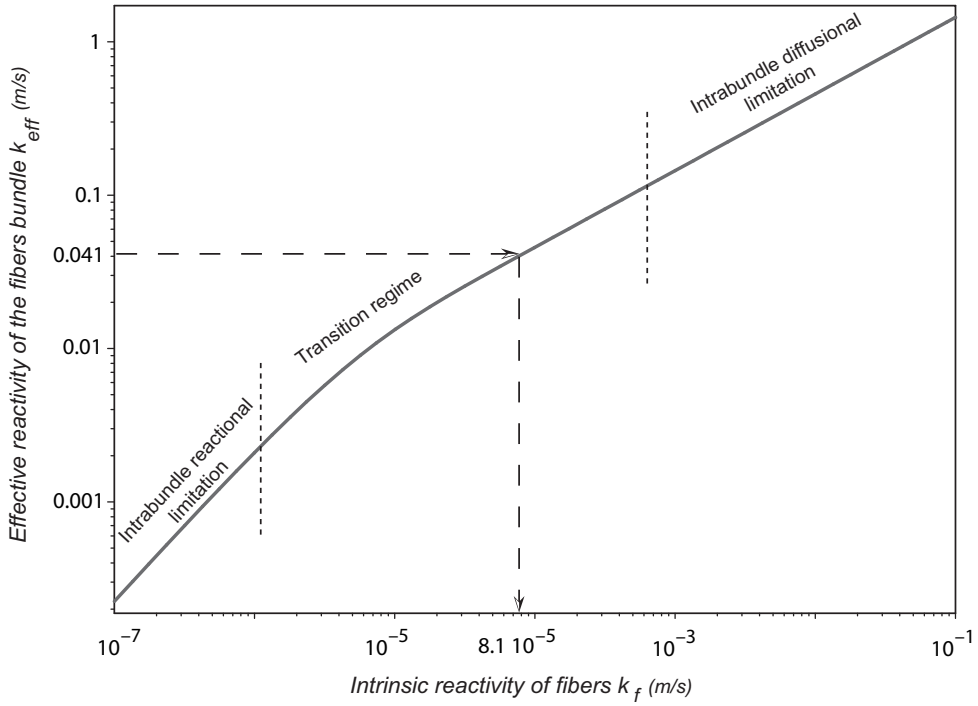


Fig. 6. Illustration of a plot of $k_{eff}$ versus $k_f$ for the fiber bundle $F4-R$

tion (11), one obtains $k_f$ as an implicit function of $k_{eff}$:

$$k_{eff} = 2\sqrt{\frac{k_f D}{\overline{d_p}}}\tanh\left(2L_f\sqrt{\frac{k_f}{\overline{d_p}D}}\right)\left(1-\frac{m_f}{L_f\rho_f S_{eff}}\right) \tag{12}$$

The table 1 is then completed using equation (12). To illustrate this equation, $k_{eff}$ is plotted versus $k_f$ for the fiber bundle properties of sample $F4-R$ on figure 6. The three reaction regimes, well known for porous media [19], are identified on this figure.

## 4 Discussion on the obtained reactivities

### *4.1 Comparison to literature data*

Because the presented method is original, it seems useful to compare the values obtained to previous results of the literature. It should be noticed that in most of the studies the oxidation rate values are not comparable to the one obtained in this study, though the units are consistent. Indeed, the oxidation rates are generally presented either under the form $r$, $j_i$, $j_s$, or, when raw mass loss rates are given, the geometrical surface of the sample is not given. I. W. Smith [10] summarized the intrinsic (geometrical) reactivities of a wide range of carbons between $580\,K$ and $2200\,K$. At $898\,K$, the reactivities, converted in the units of the present study, span between

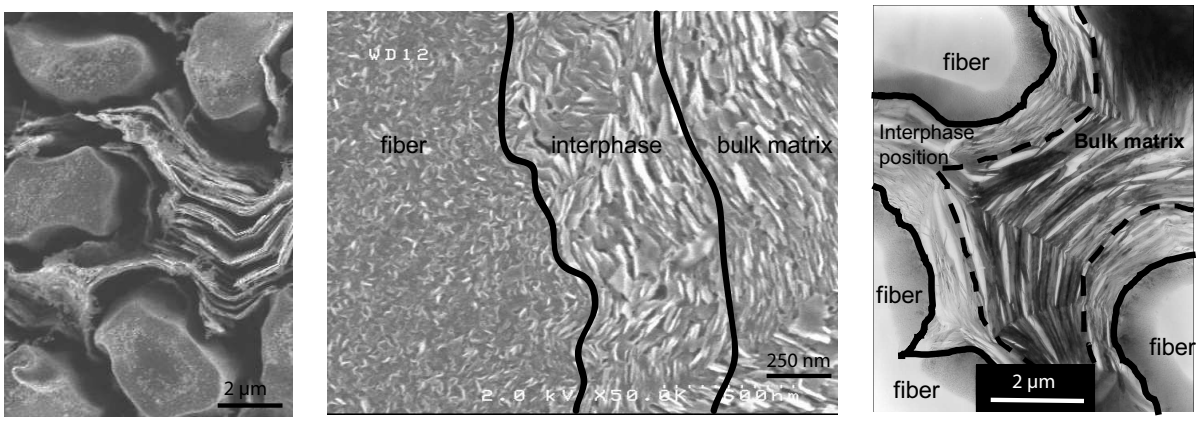


a) SEM after a short oxidation test : interphase is deeply oxidized

b) SEM of a polished slice (diamond powder 1µm) : interphase seems more disturbed

c) TEM of a thin slice : different artifacts at the interphase (due to ion-milling)

Fig. 7. Observation of the interphase lying between fibers and inter-yarn matrix (3D C/C)

$7\,10^{-6}$ and $1.3\,10^{-2}\,m.s^{-1}$. Hence, the order of magnitude of the intrinsic reactivities reported in table 1 are in agreement with this reference. A very reliable geometrical data is the radial recession velocity $v$ of an ex-PAN fiber of a 3D C/C composite treated at high temperature ($2300°C$) which has been directly measured by SEM [14] in experimental conditions close to those of the present work, the temperature being only slightly lower ($873\,K$). Its value is found to lie around $0.1\,\mu m.h^{-1}$. According to the Arrhenius law proposed in [28], the reactivity of carbon fibers at $898\,K$ is three times higher than at $873\,K$. Assuming that the regime was reaction-limited in that experiment, the resulting intrinsic oxidation rate $k_f$ is then around $3\,10^{-6}\,m.s^{-1}$ at $898\,K$, that is, it is equal to the oxidation rate of $F4-G$ which is also an ex-PAN fiber heat-treated at $2300°C$. The geometrical gasification rate of a C/C composite made of ex-PAN fibers and pitch-based matrix has been reported by Mc Kee [18] in a wide range of temperatures in experimental conditions similar to that of the present study. At $898\,K$, a fair agreement is obtained with the present 3D C/C composite.

### *4.2 Comparison between different carbons*

The oxidation resistance of the raw fibers are in the order : ex-pitch (F3-R), ex-PAN (F4-R). This should be expected from the knowledge of their degree of organization. As expected, the treatment at $1400\,°C$ leads to an important diminution of the fiber reactivity, through a diminution of catalytic effects. High temperature treatments are known to graphitize ex-PAN fibers and then lower their reactivity. The fiber $F4-G$, which is an ex-PAN fiber treated at high temperature, is therefore the most resistant. Concerning the matrices, the pyrolyzed phenolic resin ($M2$), which is poorly organized, is about three times more reactive than the ex-pitch carbonized matrix ($M1-C$). The graphitized ex-pitch matrix ($M1-G$) is roughly $3.5$ times more resistant than in carbonized state. It should be noticed that this matrix may be more representative of the matrix octets of the 3D C/C composites than of the matrix lying inside the fiber bundles. Indeed, inter and intra-bundle matrices are submitted to different conditions in terms of temperature, pressure and space occupation during graphitization. Interestingly, the actual matrix is heterogeneous : a thin matrix interphase ($0.5\,\mu m$), which lies between the fibers and

the bulk matrix, has a higher gasification rate than that of the bulk matrix. This is represented on figure 7-a for a short oxidation test. Scanning electron microscopy (SEM) micrographs have been taken on polished slices (diamond powder $1\,\mu m$) to analyze the material structure of raw composites (figure 7-b). The cohesion between the fiber and the matrix is excellent. However, close to the fiber, the matrix structure seems more disturbed. This is in accordance with the presence of a less organized and thus more reactive zone (interphase). Transmission electron microscopy (TEM) has also been carried out on a thin slice, obtained using first mechanical polishing then ion milling. Ion milling is known to generate a surface state (microcracks) susceptible to induce artifacts during TEM analysis [29]. This is observed on micrograph 7-c in bright field. An interesting fact is that artifacts are different at the interphase position. This confirms the presence of a different microstructure at the fiber/matrix interface [14, 29, 30], which plays a major role in the oxidation process [7, 14, 31, 32]. However, it is not possible to measure directly its oxidation rate since it is neither available separately nor practically extractable from the composite. A theoretical method has been proposed elsewhere to assess the interphase oxidation rate from the analysis of the steady-state surface roughness of the whole composite after oxidation [7, 9]. It is interesting to note that 3D C/C oxidation rate is definitely higher than that of its constitutive fibers ($F1$) and matrix ($M1$). This may be attributed to a weakest-link process driven by the interphase reactivity [7, 24]. As expected, 2D C/R is more reactive than 3D C/C. However, again, its reactivity is both higher than that of the fibers $F2$ and the matrix $M2$. This suggests that the behavior of this material is also complex. In this case, there is no interphase, but the pyrolysis of the phenolic resin more basically leads to a debonding between fibers and matrix that plays the same role through an enhancement of the actual geometrical surface [9].

## 5 Conclusion

The intrinsic geometrical oxidation rates of two C/C composites, of their available components, and of several carbon fibers have been measured at $898\,K$ under dry air and at atmospheric pressure. In these conditions, a diffusional limitation in the pores as well as in the bulk fluid phase was expected. In order to provide a safe method for the identification of the intrinsic reaction rates, a modeling approach associated to experimental measurements has been developed. All the samples have been inserted in a cubic crucible (the bulk materials being machined at the crucible size, the fibers being arranged in a unidirectional bundle) placed in a cylindrical oxidation reactor. The test configuration has been designed to favor a thin dynamic boundary layer above the sample, and consequently, a thin concentration boundary layer. This increases the mass transfer from the bulk fluid phase to the sample surface and lowers diffusional effects. The global scale CFD modeling of the reactor has been addressed in 3D : diffusion of the oxidant has been considered throughout the reactor in combination with convection and reaction on the sample surface. It has been shown that the overall mass transfer over the sample was unidirectional, and could be fitted by a simple analytical law in all regimes. This law has been used to extract the effective reactivity of the samples from the measured mass loss rates, which have been shown to be marred by diffusional effects. In the case of the bulk materials (composites, matrices), this effective reactivity is precisely their intrinsic geometrical reactivity. In the case

of the fiber bundles, which are porous media, a second step has been performed to extract the fiber intrinsic reactivities. The bundles have been modeled considering diffusion of the oxidant throughout the pores in combination with reaction on the fiber surface. An analytical law has been obtained: it gives the intrinsic geometrical oxidation rate of the fibers as a function of the porous media properties and of the effective oxidation rate of the bundle. Then, the corrected values of the intrinsic geometrical reaction rates, extracted from the experimental data using the models, have been compared to those of previous studies. Correct orders of magnitude are obtained. Comparing the fiber reactivities, the well-known expected tendencies have been verified as far as the fiber precursors and the thermal treatments are concerned. Moreover, the study has shown that the composite geometric reactivity was not an additive property with respect to that of its components. The behavior of the 3D C/C seems to be linked to a weakest-link process, due to the presence of a weak interphase lying between the fibers and the matrices, which has been confirmed by SEM and TEM characterizations.

## Acknowledgments

The authors wish to thank J.-F. Epherre and J.-M. Goyhénèche (CEA) for fruitful discussions, and M. Alrivie for TEM sample preparation and the SEM micrograph of figure 7-b. The authors also wish to thank CNRS and CEA for financial support, especially for a master's thesis grant to G. Bourget and a Ph. D. grant to J. Lachaud.

## References

[1] Manocha LM, Fitzer E. Carbon reinforcement and C/C composites. Springer; 1998.

[2] Bacos MP, Dorvaux JM, Lavigne O, Renollet Y. C/C composite oxidation model : I. Morphological experimental investigations. Carbon 2000;38:77–92.

[3] Duffa G, Vignoles GL, Goyhénèche JM, Aspa Y. Ablation of C/C composites: Investigation of roughness set-up from heterogeneous reactions. International Journal of Heat and Mass Transfer 2005;48(16):3387–3401.

[4] Han JC, He XD, Du SY. Oxidation and ablation of 3D carbon-carbon composite at up to 3000°C. Carbon 1995;33(4):473–478.

[5] Lachaud J, Vignoles GL, Goyhénèche JM, Epherre JF. Ablation in C/C composites: microscopic observations and 3D numerical simulation of surface roughness evolution. Ceramic Transactions 2006;191:149–160.

[6] Batt RG, Legner HH. A review of roughness-induced nosetip transition. AIAA Journal 1983; 21:7–22.

[7] Lachaud J, Aspa Y, Vignoles G, Bourget G. Experimental characterization and 3D modelling of carbon/carbon composites oxidation: role of the interphase. In: Lamon J, Torres-Marques A, editors. Proc. $12^{th}$ European Conference on Composite Materials. Biarritz, France; 2006. 8 p.

[8] Lachaud J, Aspa Y, Vignoles G, Goyhénèche JM. 3D modeling of thermochemical ablation in carbon-based materials: effect of anisotropy on surface roughness onset. Proc. $10^{th}$ International Symposium on Materials in a Space Environment. Collioure (France) : ESA Special Publication 2006, vol. 616; 10 p.

[9] Lachaud J. Simulation of ablation of carbon-based composites. Bordeaux 1 University, France. PhD thesis n°3291; 2006. In English.

[10] Smith IW. The intrinsic reactivities of carbons to oxygen. Fuel 1978;57:409–414.

[11] Dhami TL, Manocha LM, Bahl OP. Oxidation behaviour of pitch based carbon fibers. Carbon 1991; 29(1):51–60.

[12] Duvivier E. Oxidation kinetics of a C/C composite and influence on mechanical behavior. Bordeaux 1 University, France. PhD thesis n°1692; 1997. In French.

[13] Backreedy R, Jones JM, Pourkashanian M, Williams A. A study of the reaction of oxygen with graphite: Model chemistry. Faraday Discuss 2001;119:385–394.

[14] Labruquère S, Bourrat X, Pailler R, Naslain R. Structure and oxidation of C/C composites: role of the interface. Carbon 2001;39:971–984.

[15] Lahaye J, Louys F, Ehrburger P. The reactivity of carbon-carbon composites. Carbon 1990; 28(1):137–141.

[16] Vix-Guterl C, Bekri G, Dentzer J, Manocha S, Manocha LM, Ehrburger P. Reactivity in wet air of carbon-carbon composites with treated pitch. Journal of Analytical and Applied Pyrolysis 2003; 67:341–357.

[17] Lamouroux F, Camus G, Naslain R, Thebault J. Kinetics and mechanism of oxidation of 2D woven C/SiC composites: I - Experimental approach. J Am Ceram Soc 1994;77:2049–2057.

[18] McKee DW. Oxidation behavior and protection of carbon/carbon composites. Carbon 1987; 25(4):551–557.

[19] Walker PL, Rusinko F, Austin LG. Gas reactions of carbon. Advances in Catalysis and Related Subjects 1959;11:133–217.

[20] Luo R, Cheng J, Wang T. Oxidation behaviour and protection of carbon/carbon composites prepared using rapid directional diffused CVI techniques. Carbon 2002;40:1965–1972.

[21] Goto S, Han KH, Pierre GRSt. A review on oxidation kinetics of carbon fiber/carbon matrix composites at high temperature. Trans Iron Steel Inst Jpn 1986;26:597–603.

[22] Laine NR, Vastola FJ, Walker PR. The importance of active surface area in the carbon-oxygen reaction. J Phys Chem 1963;67:2030.

[23] Hippo EJ. The role of active sites in the inhibition of gas-carbon reactions. Carbon 1989;27(5):689–695.

[24] Glime WH, Cawley JD. Oxidation of carbon fibers and films in ceramic matrix composites: a weak link process. Carbon 1995;33(8):1053–1060.

[25] Chase MW. NIST-JANAF Thermochemical Tables (4th ed.). Journal of Physical Chemical Reference Data 1985; 14:1–628.

[26] Incropera FP, De Witt DP. Fundamentals of Heat and Mass Transfer. 5th ed. John Wiley and Sons; 2002.

[27] Transvalidou F, Sotirchos SV. Effective diffusion coefficients in square arrays of filament bundles. AIChE J 1996;42(9):2426–2438.

[28] Drawin S, Bacos MP, Dorvaux JM, Lavigne O. Oxidation model for carbon-carbon composites. Proc. 4th International Aerospace Planes Conference. Orlando(Florida, USA): AIAA paper, 1992; 9 p.

[29] Dumont M. 3D C/C composites densified by mesophase pitch impregnation/carbonization. Bordeaux 1 University, France. PhD thesis n°2344; 2001. In French.

[30] Oberlin A, Goma J, Rouzaud JN. Techniques d'étude des structures et texture (microtextures) des matériaux carbonés. J Chimie Physique 1984;81(11):701–710.

[31] Rodriguez-Mirasol J, Thrower PA, Radovic LR. On the oxidation resistance of carbon-carbon composites: importance of fiber structure for composite reactivity. Carbon 1995;33(4):545–554.

[32] Guo W, Xiao H, Yasuada E, Cheng Y. Oxidation kinetics and mechanisms of a 2D-C/C composite. Carbon 2006;44:3269–3276.

## List of Figures



## List of Tables